Faf1 accelerates p97-mediated protein unfolding by promoting ubiquitin engagement

Zengwei Liao[1,2,3], Connor Arkinson[1,2,3], and Andreas Martin[1,2,3,4*]

Affiliations:

[1]California Institute for Quantitative Biosciences, University of California at Berkeley, Berkeley, CA 94720, USA

[2]Department of Molecular and Cell Biology, University of California at Berkeley, Berkeley, CA 94720, USA

[3]Howard Hughes Medical Institute, University of California at Berkeley, Berkeley, CA 94720, USA

[4] Lead contact

*Correspondence: a.martin@berkeley.edu

Summary

P97/VCP is a protein unfoldase of the AAA+ ATPase family that plays essential roles in numerous cellular processes, including ER-associated degradation and DNA replication. P97 utilizes various cofactors to process different substrates. For unfolding of proteins that are modified with K48-linked ubiquitin chains, p97 works with the heterodimeric cofactor Ufd1-Npl4, and the cofactor Faf1 was shown to enhance this activity in the context of replisome disassembly, yet the underlying mechanisms remain unknown.

Here, we employ an *in vitro* reconstituted system with human components for biochemical experiments, mutational studies, FRET-based assays, and cryo-EM structure determination to reveal that Faf1 plays a generic role in accelerating ubiquitin-dependent substrate processing by promoting the unfolding of an initiator ubiquitin and its engagement by the ATPase motor. Faf1 thereby uses its p97-bound C-terminal UBX domain to anchor a long helix that braces the UT3 domain of Ufd1 and apparently stabilizes the Ufd1-Npl4 cofactor for ubiquitin unfolding. Our findings demonstrate how p97 works simultaneously with several cofactors to facilitate the unfolding of ubiquitinated proteins, indicating more complex regulatory mechanisms for substrate selection than for the simpler Cdc48 ortholog in yeast.

Introduction

The mammalian Valosin-Containing Protein (VCP) or p97 (Cdc48 in yeast) is an essential AAA+ (ATPases Associated with various cellular Activities) protein unfoldase that plays roles in many cellular processes, such as endoplasmic reticulum-associated degradation (ERAD), endosomal trafficking, membrane fusion, DNA damage response, and DNA replication [1-6]. A major function of p97 is to extract proteins from macromolecular complexes or membranes and unfold them prior to degradation by the 26S proteasome[7]. Many of p97's substrates are therefore marked with polyubiquitin chains. Mutations in p97 are for instance linked to cardiovascular and neurodegenerative diseases, including multisystem proteinopathy (MSP), a fatal disease with various clinical pathologies that affect the brain, muscle, and bone[8-10].

P97 is a homo-hexamer with each protomer containing a N-terminal domain (NTD) and tandem ATPase domains, D1 and D2, that in the hexamer form stacked rings. Many cofactor proteins bind p97 to contribute various activities or regulate its function, including substrate recruitment, engagement, unfolding, and deubiquitination[11]. Cofactors thereby use ubiquitin regulatory X (UBX/UBXL) domains or linear sequences such as VCP-binding motifs (VBMs), VCP-interacting motifs (VIMs), or SHP (Src homology region 2 domain-containing phosphatase) motifs to interact with p97's NTD, while others bind the C-terminal tail of p97 through a PUB (peptide:N-glycanase and UBA or UBX-containing proteins) or PUL (PLAP, Ufd3p, and Lub1p) domains. One of the most well studied p97 cofactors is the heterodimeric Ufd1-Npl4 (UN) complex, which binds on top of the p97 hexamer, recruits ubiquitinated substrates, and initiates their unfolding, with specificity for K48-linked ubiquitin chains[12,13]. Npl4 interacts through its UBXL and zinc-finger domains with p97's NTD and D1 domains, while Ufd1 contacts Npl4 through a small interface and is highly flexible, which so far prevented its visualization by cryo-EM[12]. Structural and functional analyses of UN-bound Cdc48 indicate that an initiator ubiquitin in the substrate-attached ubiquitin chain gets unfolded by UN in an ATP independent manner and binds in a hydrophobic groove on Npl4 to insert its N-terminus into the Cdc48 central channel. The Cdc48 motor then utilizes ATP hydrolysis to engage and pull on the initiator ubiquitin, unfold and translocate any proximal ubiquitin moieties in the chain, and thread the attached substrate protein itself[12,14]. The ubiquitin moiety immediately distal to the initiator was observed to interact with parts of Npl4 and Ufd1, while

the consecutive next two ubiquitins bind on top of the so-called tower domain of Npl4[12,15] and increase substrate affinity during recruitment[14]. Importantly, the ubiquitin moiety on the proximal, substrate-facing side of the initiator binds Ufd1's UT3 domain, which appears to determine the K48-ubiquitin linkage specific of Cdc48-UN and is critical for insertion of the initiator ubiquitin into the ATPase motor[14].

Interestingly, only the proximal ubiquitin(s) and the substrate are unfolded and threaded, whereas ubiquitins on the distal side of the initiator are not unfolded[14,16-18]. Release of the ubiquitinated substrate from the motor after unfolding therefore represents the rate-limiting step, at least in the absence of other cofactors or deubiquitinases, and while Cdc48-UN let go of its substrates to allow multiple-turnover unfolding in vitro[14], p97-UN appears to get stuck after a single substrate-unfolding event[18]. Furthermore, without any additional cofactors, p97-UN is far less efficient in substrate unfolding and requires much longer ubiquitin chains[19,20], indicating more complex regulatory mechanisms for substrate recruitment and processing.

In humans there is an expanded family of p97 cofactors, but it remains unclear how, when, or which of these cofactors work together. Many of them may act independently, compete for the same binding sites on p97, or function only in the context of specific substrates. However, recent insights into replisome disassembly showed that fas-associated factor 1 (Faf1), works with p97-UN to enhance the unfolding of MCM complexes and their removal from DNA, potentially through lowering the threshold for the ubiquitin-chain length[19]. Interestingly, in addition to replisome disassembly[19,21], Faf1 has been reported to play significant roles in other pathways, including immune response[22,23] and aggresome clearance[24], indicating possible generic roles in multiple p97-dependent processes.

Faf1 is a multidomain protein that uses it's C-terminal UBX domain for binding to p97's NTD [25], potentially interacts with ubiquitin chains through its N-terminal UBA (ubiquitin-associated) domain[26], and contacts other chaperones, like Hsp70, through one of its two UBL domains[27]. However, the mechanism for Faf1-mediated enhancement of substrate unfolding by p97-UN remains unclear.

Here, we *in vitro* reconstitute p97-UN unfolding of model substrates with K48-linked ubiquitin chains and reveal that Faf1 has a generic function by facilitating initiation, increasing substrate capture, and thus accelerating processing. Our FRET-based studies show that Faf1

specifically accelerates initiator-ubiquitin insertion into p97, with rates that are comparable to those of Cdc48-UN. Interestingly, p97 subsequently unravels the mEos model substrate much more slowly than Cdc48, suggesting mechanical unfolding as the rate-limiting step for p97. Using cryo-EM single-particle analysis, we observe that Faf1's UBX domain binds to the NTD of p97 and stabilizes the SHP motif of Ufd1, which is key to Faf1 recruitment. In addition, through AlphaFold modelling and site-specific mutagenesis, combined with our substrate-unfolding and FRET-based assays, we determine that Faf1 uses a helix preceding its C-terminal UBX domain to bind and stabilize the dynamic UT3 domain of Ufd1, thereby allowing for more efficient initiator-ubiquitin unfolding and insertion into p97. Finally, we show that this mechanism is conserved for the membrane associated cofactor Faf2, which plays critical roles in ERAD[28,29]. Faf1 and Faf2 promote a more productive complex between UN, p97, and ubiquitinated substrates that allows higher efficiency in ubiquitin insertion and unfolding initiation, which indicates how those cofactors may generically support the numerous cellular functions of p97-UN.

Results

Faf1 stimulates unfolding activity of p97-UN

To test whether Faf1 can generally accelerate the unfolding of ubiquitinated substrates by p97-UN, we utilized a photoconverted, red-fluorescent and thus irreversibly unfolding mEos3.2 model substrate with a covalently fused mono-ubiquitin that was enzymatically extended into long (> 8 moieties) K48-linked polyubiquitin chains (Fig. S1A,B)[30,31]. Human p97, UN, and Faf1 were recombinantly expressed and purified from *E.coli* (Fig. 1B). Reconstituted Eos-unfolding experiments under single-turnover conditions (i.e. enzyme at saturating concentrations and in excess over substrate) in the absence or presence of Faf1 showed that Faf1 accelerates p97-UN-mediated substrate processing by ~ 5-fold, from $\tau_{Eos\ unfold}$ (-Faf1) = 4727 ± 688 s to $\tau_{Eos\ unfold}$ (+Faf1) = 902 ± 76 s (Fig. 1C, Fig. S1C). These results are overall consistent with previous findings about the Faf1 effects on MCM-complex disassembly[19], but, importantly, also demonstrate a role in accelerating unfolding of ubiquitinated substrates in general[19].

Faf1 UBX-domain interactions with p97 NTD are essential for stimulating unfolding

For gaining structural insights into Faf1's stimulating effects on p97 unfolding activity, we aimed to capture a substrate-engaged p97-UN-Faf1 complex. We initiated the unfolding reaction with ATP, then switched through buffer-exchange to the non-hydrolyzable ATPγS analog in order to stall substrate-engaged complexes (Fig. S1E,F), and analyzed the sample by cryo-EM. Although SDS-PAGE after size-exclusion chromatography confirmed that we isolated a stable complex containing all components (Fig. S1F), the single-particle cryo-EM analysis resolved only the p97 hexamers with no defined density for most of Faf1, the UN complex, or the substrate, likely due to high flexibility and strong conformational heterogeneity. Symmetry expansion and focused classification of individual p97 promoters with a mask on the NTD (Fig. 2A, Fig. S2) identified ~ 32 % of particles with extra NTD-bound density, 16 % of which were further refined and showed sufficiently high resolution (3.27 Å) for modeling the UBX domain of Faf1 (Fig. 2B, Table 1). This UBX-domain interaction with p97's NTD is consistent with previous crystal structures[32,33], but we also partially resolved a long Faf1 helix (FH) that precedes the UBX domain and extends up from the NTD (Fig. 2B). Additional density was observed on the opposite side of the same NTD, and we turned to AlphaFold predictions with a truncated p97 (ΔD2 domain), UN, and Faf1 to determine its identity (Fig. 4A, S6A). The predicted complex structures showed high-confidence UBX-NTD binding, in agreement with our structural data, and in addition allowed us to model a fragment of Ufd1's SHP loop, which is anchored through L235 to a hydrophobic hole on p97's NTD (Fig. 2C). Although this SHP-NTD interaction was identified before[34,35], it is exciting to observe that Ufd1 and Faf1 interact simultaneously with the same NTD of the hexamer, indicating potential cooperativity in binding. Determining a possible cooperativity is difficult due to the multivalent interactions between Npl4, Ufd1, and Faf1, and the fact that the SHP motif is critical for Ufd1 binding in the absence and presence of Faf1, such that point mutations in this motif lead to vital defects in substrate-unfolding activity. Interestingly, we only observed binding of Faf1's UBX domain to p97 NTDs that were in the "up" conformation. The NTDs can adopt "up" or "down" conformations depending on the nucleotide sate of the D1 ATPase domain [36], and the up conformation is preferentially bound by UN[18,37], which may further stabilize this state and thus favor Faf1 UBX-domain binding to cooperatively form a ternary complex. These cryo-EM data, together with

the apparent stoichiometries observed by SDS PAGE (Fig. S1F), indicate a 1:1:1 complex of Faf1, UN, and p97 hexamer.

To assess which parts of the multi-domain Faf1 are responsible for the stimulation of p97 unfolding, we generated several truncated variants and tested their effect on both substrate unfolding and ATP hydrolysis by p97 (Fig. 2D, S1D). Faf1 alone, in the absence of UN and substrate, did not increase p97's very low basal ATPase activity. However, Faf1 stimulated ATP hydrolysis ~ 1.7-fold in the presence of substrate and UN, suggesting that it either accelerates the motor during threading and unfolding or it facilitates substrate engagement and thus increases the fraction of actively substrate-processing p97 that has a higher ATP-hydrolysis rate than idling p97 in the absence of substrate [18]. While Faf1's UBA and UBL domains were dispensable for p97 activation, deletion of its UBX domain abolished Faf1's stimulatory effects (Fig. 2E-F), which is consistent with previous observations for p97-mediated replisome disassembly in the presence of Faf1[19]. Faf1's two UBL domains were suggested to function in binding other chaperones, such as Hsp70, and thus may play context-specific roles[23,27], similar to the UAS domain that appears to bind fatty acids [38]. We found that a minimal C-terminal fragment consisting of the FH and UBX domain (FH-UBX) leads to a stimulation of p97's unfolding activity that is comparable to that of full-length Faf1, whereas the UBX domain alone was insufficient for stimulation (Fig. 2E). In the AlphaFold model of the complex structure, the UT3 domain of Ufd1 binds to Faf1's FH that protrudes from the UBX domain. Since the UT3 domain binds the ubiquitin moiety proximally neighboring the initiator ubiquitin in a substrate-attached ubiquitin chain[14], we postulate that an interaction with the rigid, UBX-NTD-anchored FH stabilizes the UT3 domain above p97 for a more productive initiator unfolding by Npl4 and insertion into the motor, leading to an apparently higher rate of substrate unfolding.

Faf1 promotes ubiquitin insertion and engagement by p97

To test whether the FH-UT3 domain interaction is critical for the Faf1-mediated stimulation of substrate unfolding through a potential acceleration of initiator-ubiquitin insertion, we employed a FRET-based initiation assay that we previously developed for Cdc48-UN [14]. For this assay, the second ubiquitin in unanchored long (> 10) ubiquitin chains was labeled on an

engineered cysteine near its N-terminus with a fluorescent donor dye (Cy3). P97 subunits were labeled with an acceptor dye (LD655) on the unnatural amino acid azido-phenylalanine (AzF) that was introduced in place of D592, located near the exit of the central channel (Fig. 3A). Unfolding and threading of the donor-labeled ubiquitin is thus expected to bring it into proximity of the acceptor label and increase the apparent FRET efficiency. Control experiments confirmed that p97 with incorporated AzF and LD655 labels had unfolding activity, albeit at a reduced level compared to the unmodified enzyme (Fig. S3A-C). Measurements of fluorescence spectra after mixing the Cy3-labeled ubiquitin chains with ^{LD655}p97-UN and ATP in the absence of Faf1 showed no difference in donor or acceptor fluorescence compared to the isolated components, whereas the presence Faf1 caused significant reciprocal changes in fluorescence intensities that are indicative of FRET (Fig. 3B). Faf1 thus appears to stimulate initiator-ubiquitin unfolding and insertion into the central channel, whereas UN alone is too inefficient for a considerable signal change over the time frame of this FRET assay, even though it can support slow substrate processing in our unfolding assay (Fig. 1C).

It is important to note that the changes in donor and acceptor signals were stable for an extended amount of time (> 10 min), suggesting that the ubiquitin chain stalls in p97, with the labeled second ubiquitin likely located inside or below the exit of the central channel, in proximity to the acceptor dye. This indicates p97's inability to unfold and translocate the distal part of the ubiquitin chain, or otherwise release it, for instance through lateral opening of the hexameric ring, despite the presence of ATP in our assay. This is in contrast to Cdc48-UN, which in this assay required the use of the non-hydrolyzable analog ATPγS for a stable FRET signal after initiator-ubiquitin insertion. Consistent with these observations is that Cdc48-UN can catalyze multiple-turnover substrate unfolding in the presence of ATP [14], with substrate release as the rate-limiting step, whereas p97-UN only supports single-turnover unfolding and gets stuck on the distal part of the ubiquitin chain, at least in a minimal reconstituted system without the 26S proteasome, deubiquitinases, or potentially ring-opening cofactors like UBXD1[39]. UN-mediated initiator-ubiquitin unfolding and insertion into Cdc48 was found to be fast (~ 3 s) even in the presence of ATPγS [14], whereas p97-UN required ATP hydrolysis for a signal change in our initiation assay (Fig. S3D,E). It is possible that p97 depends on a combination of ATP- and ADP-bound subunits in the hexamer to adopt an appropriate spiral-

staircase conformation for ubiquitin insertion, or that Cdc48's much higher ATP-hydrolysis activity allows it to hydrolyze some ATPγS and get into the right staircase state for initiation. Alternatively, an initiator ubiquitin may be able to insert into ATPγS-bound p97, but the long chains necessary for efficient initiation by human p97-UN may strongly reduce the probability that the second, donor-labeled ubiquitin is chosen as the initiator. Initiation at any position higher-up in the chain would therefore require ATP-hydrolysis-driven unfolding and translocation of the proximal part of the chain to move the labeled ubiquitin 2 through the pore and into proximity of the acceptor for a FRET signal change (Fig. S3F).

Using the double mutations W241A/R242E or E446K/Y447A in the ubiquitin-binding groove of Npl4[12,14], we confirmed that initiator-ubiquitin insertion into p97 still depended on its interaction with the Npl4 groove, even in the presence of Faf1 (Fig. S3G). In agreement with our findings for substrate unfolding, FRET-based initiation assays with truncated Faf1 variants showed that the UBX domain is critical for p97 binding and that the minimal FH-UBX domain fragment is sufficient for accelerating ubiquitin insertion into the central channel of p97 (Fig. 3C).

Despite the presence of Faf1, unfolding of the ubiquitinated Eos substrate by p97-UN is ~ 200 times slower than by Cdc48-UN (Fig. 1C) [14]. To assess potential differences in the kinetics of unfolding initiation, we monitored the FRET changes upon ubiquitin insertion into p97-UN-Faf1 in stopped-flow mixing experiments. Interestingly, ubiquitin insertion occurred with an apparent time constant of $\tau_{initiation}$ = 5.1 ± 0.2 s (Fig. S3H), similar to Cdc48-UN ($\tau_{initiation}$ = 3.2 ± 0.1 s [14]). The velocity of substrate unfolding by p97-UN-Faf1 under single-turnover conditions is therefore not limited by slow initiation or the distinct ubiquitin-chain length requirements of p97-UN compared to Cdc48-UN, but due to slow Eos unfolding itself. To confirm that p97 does not get stuck on Eos, we used an Eos-Turquoise fusion substrate. The observed loss in Turquoise fluorescence confirmed that Eos is completely unfolded and threaded by p97, albeit very slowly (Fig. S4A). The significant difference in substrate-unfolding speeds for p97 and Cdc48 ($\tau_{Eos\ unfold}$ = 901.5 ± 75.6 s and $\tau_{Eos\ unfold}$ = 4.4 ± 0.1 s, respectively) may originate from the almost two orders of magnitude different ATP-hydrolysis activities (16 min^{-1} for p97 versus ~ 1000 min^{-1} for Cdc48 in the absence of UN and substrate [14,20]). Furthermore, p97 may have extra layers of negative regulation that could be encoded through sequence differences or

additional cofactors. Assuming that Faf1 primarily facilitates the unfolding and insertion of the initiator ubiquitin, we can use the observed time constants for Eos processing in the absence versus presence of Faf1 ($\tau_{Eos\ unfold}$ (-Faf1) = 4727 ± 688 s and $\tau_{Eos\ unfold}$ (+Faf1) = 902 ± 76 s) together with the time constant for initiation with Faf1 from the FRET-based assay ($\tau_{initiation}$ = 5.1 ± 0.2 s) to estimate that Faf1 accelerates initiation by more than 700 fold, likely by stabilizing a more productive UN complex above p97. Subsequent unfolding of the Eos moiety in our model substrate occurs much more slowly and becomes rate-limiting, accounting for ~ 20% of the time spent on substrate processing, which explains the maximum 5-fold overall acceleration by Faf1, despite its major effects on the efficiency and velocity of initiation.

Faf1 does not enhance the activity of p97 bound to yeast UN

Since there are clear differences between human and yeast UN, we wondered whether human UN is more dynamic and therefore depends on Faf1 to form a productive complex for unfolding initiation. Interestingly, yeast UN (yUN) can support p97 unfolding of the ubiquitinated-Eos substrate at a rate of τ_{Eos} 26.7 ± 2.4 min, which is ~ 3.5-fold higher than the rate in the presence of human UN (hUN) without Faf1 (Fig. S4B) and demonstrates the functional conservation of the AAA+ motors. The addition of full-length Faf1 did not further stimulate the unfolding activity of p97-yUN, but in fact reduced it (Fig. S4B), potentially because Faf1's UBL domains bind to the tower ubiquitin-binding sites of the yeast Npl4. We therefore used the FH-UBX domain fragment of Faf1 and observed an unfolding activity that was comparable to that of p97-yUN (Fig. S4B). yUN may intrinsically encode for more productive ubiquitin unfolding and insertion into Cdc48 or p97, whereas hUN is potentially more dynamic and dependents on a stabilization of Ufd1's UT3 domain through interactions with Faf1's FH-UBX-domain portion.

The stimulatory helix interaction with Ufd1's UT3 domain is conserved for Faf2

Truncation of Faf1's FH abolished Faf1's stimulatory effects on substrate unfolding activity (Fig. 2E), consistent with our model that FH stabilizes Ufd1's UT3 domain. Yet to further validate this hypothesis and the AlphaFold-predicted structure of the ternary complex, we sought out point mutations in Faf1 and Ufd1 that sterically break the binding interface. Indeed, the S518K mutation in Faf1 or the A140E mutation in Ufd1 abolished the accelerated substrate

unfolding by p97-UN-Faf1 (Fig. 4A-C), yet A140E did not affect substrate unfolding in the absence of Faf1 (Fig. 4B).

Faf2 is a membrane-associated cofactor that is involved in ERAD[28,29], but shows partial conservation with Faf1 (Fig. S5). AlphaFold predicts that Faf2's C-terminal UBX domain interacts with p97's NTD, while the preceding FH binds to Ufd1's UT3 domain (Fig. 4D). We generated two truncated Faf2 fragments, with deletions of the first 271 residues, which leaves the C-terminal helix and UBX domain, or 296 residues, which in addition removes about half of the predicted UT3-binding region of the helix and represents a fragment previously used in replisome-disassembly studies (Fig. 4D-E, S1D). In our Eos unfolding assays, the addition of Faf2$^{\Delta 1\text{-}271}$ to p97-UN led to a 5-fold stimulated activity (Fig. 4F), comparable to the FH-UBX domain fragment of Faf1. In contrast, Faf2$^{\Delta 1\text{-}296}$ has some of the UT3-interacting residues removed and failed to accelerate substrate turnover. In summary, these results suggest that the helix preceding the UBX domain in both Faf1 and Faf2 interacts with the UT3 domain of Ufd1 to stimulate substrate processing by p97-UN, likely by stabilizing Ufd1's position for more productive initiator-ubiquitin unfolding and insertion into the AAA+ motor.

Discussion

Here we show that Faf1 and Faf2 accelerate the early steps in the processing of ubiquitinated substrates by p97-UN. The effects depend on the recruitment of these cofactors through their UBX domain to the upward conformation of p97's NTDs, which positions a conserved helix upstream of the UBX domain to interact with the UT3 domain of Ufd1. This interaction appears critical for promoting a productive p97-UN complex that can rapidly insert the initiator ubiquitin into the ATPase motor, likely through stabilizing the position of Ufd1's UT3 domain relative to Npl4. Since the UT3 domain binds the ubiquitin moiety that proximally neighbors the initiator ubiquitin, this UT3-domain stabilization may facilitate the recruitment of the initiator ubiquitin, its unfolding, and/or its placement in Npl4's hydrophobic groove for p97 insertion. Also, ubiquitin unfolding and insertion critically depend on anchoring Ufd1 through its SHP motif on p97's NTD, and binding of the same NTD by the UBX domain of Faf1 or Faf2 likely further stabilizes this interaction. In contrast to Cdc48-UN-substrate complexes, structural analyses of p97 complexes appear much more challenging, and neither UN nor Faf1 or the substrate

could be visualized in our cryo-EM maps, perhaps due to higher intrinsic flexibility of the human system.

We observed ~ 5-fold faster kinetics of substrate processing by p97-UN in the presence of Faf1, even though Eos unfolding is by far the rate-limiting step and Faf1 appears to accelerate only the initiation. This is because initiation by p97-UN in the absence of Faf1 is highly inefficient and therefore becomes apparently rate-determining. Unlike Cdc48-UN, which shows maximum initiation and substrate-unfolding rates with ubiquitin chains of 6 moieties and reasonable activities even with dimeric chains[14], p97-UN requires much longer ubiquitin chains for any detectable unfolding activity[19]. Our findings that Faf1 strongly facilitates ubiquitin engagement thus explain previous reports about Faf1 lowering the chain-length threshold for p97-UN[19]. Directly bridging p97's NTD and Ufd1's UT3 domain through interactions with Faf1's UBX domain and rigid helix thereby seem essential, and it is conceivable that other UBX-domain containing proteins use similar multivalent contacts to help coordinate the myriad of p97 cofactors. Interestingly, Faf1 contains several other domains, including a ubiquitin-binding UBA domain[26] whose truncation did not cause significant defects in our unfolding experiments. Faf1 may thus engage in other substrate-specific interactions[23,27] or even function in other pathways[38,40].

Initiation by p97-UN in the presence of Faf1 occurs similarly fast as by Cdc48-UN, yet unfolding the Eos moiety of our model substrate takes p97 ~ 200 fold longer than Cdc48. This is likely caused by the vastly different rates in ATP hydrolysis for these human and yeast orthologs. Previous studies of GFP degradation by the bacterial AAA+ protease ClpXP showed that successful unfolding of the beta-barrel structure critically depends on the pulling frequency of the motor[41], such that p97 may have a considerable disadvantage in unraveling Eos and potentially have to compete with the fast refolding of a short-lived unfolding intermediate. Future studies will have to address whether p97 could benefit in its substrate-unfolding velocity from other cofactors that either stimulate ATP-hydrolysis or act as chaperones to destabilize the folded domains of substrate proteins.

Resource availability

Lead contact

Further information and requests for resources and reagents should be directed to and will be fulfilled by the lead contact, Andreas Martin (a.martin@berkeley.edu).

Materials availability

All constructs generated in this study are available from the lead contact upon request and completion of a Material Transfer Agreement.

Data and Code Availability:

- All data generated or analyzed during this study are included in this manuscript and the Supplemental materials. The cryo-EM density map and corresponding atomic coordinates for the resolved portions of the human p97-UN-Faf1 complex can be found on the Electron Microscopy Data Bank (EMDB) with the accession code EMD-73536 and on the Protein Data Bank (PDB) with the accession code PDB-9YW2.
- This paper does not report original code.

Any additional information required to reanalyze the data reported in this paper is available from the lead contact upon request.

Acknowledgements:

We thank the members of the Martin lab for helpful discussions. We also thank Rui Yan and Shixin Yang at the HHMI Janelia CryoEM Facility for help in microscope operation and data collection.

Funding:

This research was funded by the Howard Hughes Medical Institute (Z.L., C.A., A.M.) and by the US National Institutes of Health (R01-GM094497 to A.M.).

Author Contributions:

Conceptualization, Z.L. and A.M.; Methodology, Z.L., C.A., and A.M.; Investigation, Z.L. and C.A.; Writing – Original Draft, Z.L. and A.M.; Writing – Review & Editing, Z.L., A.M., and C.A.; Funding Acquisition, A.M.; Supervision, A.M.

Declaration of Interests:

The authors declare no competing interests.

Methods

Purification of recombinant proteins

Expression, purification, and labeling of p97 and $p97^{D592AzF}$ were carried out as previously described[20,42]. Briefly, after the recombinant expression of wild-type p97 in *E. coli*, cells were harvested by centrifugation at 3,500 rcf and resuspended in NiA buffer (50 mM HEPES-KOH, pH 7.6, 500 mM KCl, 20 mM imidazole) supplemented with benzonase nuclease, lysozyme, and protease inhibitors. Cells were lysed by sonication, the lysate was clarified by centrifugation at 27,000 rcf, and the supernatant was loaded onto Ni-NTA resin followed by 10 column volumes (CV) washing with NiA buffer. The protein was eluted with NiB buffer (50 mM HEPES, pH 7.6, 500 mM KCl, 400 mM imidazole) and concentrated before loading on a size-exclusion chromatography column (HiLoad Superdex 200 16/60) that was equilibrated with GF buffer (50 mM HEPES-KOH, pH 7.6 150 mM KCl, 5 mM $MgCl_2$, 1 mM DTT). Fractions were analyzed by SDS-PAGE, concentrated, and snap frozen by liquid nitrogen. For $p97^{D592AzF}$ expression, cells were co-transformed with the plasmids coding for $p97^{D592AzF}$ and the AzF-tRNA synthetase, grown at 37°C to an OD_{600} of 0.6, and incubated with AzF at a final concentration of 1 mM. After 30 min, expression was induced with 0.5 mM IPTG and cells were grown at 18°C for 16 h before harvest.

Expression and purification of human UN complex and mutans were carried our as previously described[20]. Briefly, *E. coli* BL21 DE3 cells with a plasmid coding for Ufd1 or Npl4 were grown separately and resuspended in NiA buffer together before cell lysis. The supernatant after centrifugation was subjected to Ni-NTA purification and UN was further purified by size-exclusion chromatography (HiLoad Superdex 200 16/60). Peak fractions containing the UN complex were pooled and concentrated before snap freezing.

Faf1, Faf2, and their variants were expressed in Rosetta2 pLysS cells as GST fusions with an HRV-3C protease cleavage sites. Cells were lysed, clarified by centrifugation, and loaded on a glutathione resin equilibrated with GF buffer. After washing with 20 CV of GF buffer, GST-HRV3C protease was added to the resin and incubated at 4°C overnight to cleave off the tag. Cleaved target proteins were washed off from the resin with GF buffer supplemented with 5 mM DTT and further purified by size exclusion chromatography (Superdex 200 increase 10/300).

Wild-type human ubiquitin and its variants were purified as previously reported[14]. In brief, for wild-type ubiquitin and ubiquitin with a N-terminal Met-Cys extension (MC-Ub), cells were lysed in NiA buffer, the supernatant was clarified by centrifugation at 27,000 rcf for 30 min, and glacial acetic acid was gradually added until the solution reached a pH of ~ 4.5. Precipitants were separated by centrifugation at 27,000 rcf for 30 min, the supernatant was dialyzed at 4°C for 16 h against 50 mM sodium acetate buffer, pH 4.5, and additional precipitants were removed by centrifugation. The supernatant was loaded to a cation-exchange column (5 mM HiTrap SP HP, Cytiva) equilibrated with 50 mM sodium acetate buffer, pH 4.5, and proteins were eluted with a linear gradient of 1-60 % of 1 M NaCl over 30 CV. Peak fractions containing the target protein were pooled and concentrated, and proteins were further purified by size exclusion chromatography (HiLoad Superdex 75 16/60) in GF buffer. For Ub-His and MC-Ub-His, a Ni-NTA purification step was performed instead of the acidic precipitation process. For all MC-Ub variants, 5 mM DTT was added to the GF buffer for the final size exclusion chromatography to keep cysteines reduced.

The plasmid for expression of His-SUMO-Ub^{G76V}-mEos3.2 was synthesized by GenScript and used to transform BL21 Star (DE3) competent cells. Expression was induced at OD_{600} = 0.6, and cell were grown at 20°C for 16 h before harvest. After pelleting, cells were resuspended in NiA buffer and lysed by sonication. The lysate was cleared by centrifugation and the supernatant was loaded on Ni-NTA resin pre-equilibrated with NiA buffer. After washing with 20 CV NiA buffer, the target protein was eluted with NiB buffer. Imidazole in the solution was diluted using Amicon spin filters before the addition of SENP2 protease. The cleavage was performed at 4°C for 16 h, and cleaved Eos was isolated as the flow through fraction of a subtractive Ni-NTA purification. Samples were concentrated and further purified by size-exclusion chromatography (HiLoad Superdex 75 16/60).

For the fusion protein of Eos-Turquoise, BL21Star (DE3) competent cells were transformed with pET24 His-3C-Ub^{G76V}-mEos3.2-Turqoise and grown as described above. The protein was purified by Ni-NTA affinity in NiA buffer and size-exclusion chromatography in GF buffer with the His tag uncleaved.

Mouse E1 (Ube1)[43] and the E2-E3 chimera gp78RING-Ube2g2[20] were expressed and purified as described.

Protein labeling with fluorophores

After Ni-NTA affinity purification, $p97^{D592AzF}$ was treated with 5-fold molar excess of DTNB for 30 min at room temperature to protect solvent-exposed cysteines and then labeled with 5-fold molar excess of LD655-DBCO (custom synthesis by Lumidyne Technologies) for 2 h at room temperature. The reaction was quenched with an excess amount of free AzF and treated with 5 mM DTT before a final purification by size exclusion chromatography (HiLoad Superdex 200 16/60) in GF buffer. The efficiency of labeling was estimated based on the protein concentration measured by BCA assay in comparison with LD655 absorbance (typically 20-30%).

MC-Ub and its variants were labeled with Cy3- or Cy5-maleimide dyes at the N-terminal engineered cysteine. First, MC-Ub was treated with 1 mM TCEP for 30 min at room temperature, followed by the addition of 10-fold molar excess of sulfo-Cy3-maleimide or sulfo-Cy5-maleimide (Lumiprobe) dissolved in DMSO. The final concentration of MC-Ub was 500 μM, and the labeling reactions were carried out at room temperature for 30 min. Reactions were quenched by adding DTT to a final concentration of 10 mM, the protein was concentrated and subjected to size-exclusion chromatography (Superdex 75 increase 10/300) in GF buffer. Protein concentration was estimated based on Cy3 or Cy5 absorbance.

Preparation of ubiquitinated Eos and Eos-Turquoise substrates

The reaction mixture for ubiquitination consisted of 7.5 μM E1, 125 μM chimeric E2-E3, 100 μM Ub^{G76V}-mEos3.2 or Ub^{G76V}-mEos3.2-Turquoise, 500 μM ubiquitin and GF buffer with 10 mM ATP. The reaction was carried out in a total volume of 500 μL at 37°C for 2.5 h. An extra 500 μM ubiquitin was added every 30 min to efficiently elongate the ubiquitin chain. The mixture was subsequently subjected to size-exclusion chromatography (Superose 6 increase 10/300), and fractions with substrate-attached ubiquitin chain of more than 10 Ub were pooled and concentrated. To prepare the red Eos, purified ubiquitinated green Eos was photoconverted on ice for 30 min using a 395nm 50W LED Black Light lamp (CONALUX). The conversion efficiency was ~ 50-60% based on the fluorescence ratio.

Assembly of ubiquitin chains

To prepare Ub-^{Cy3}Ub-Ub$_n$ and ^{Cy5}Ub-^{Cy3}Ub-Ub$_n$ chains used for FRET-based experiments, the first step was to make Ub-His-^{Cy3}Ub and ^{Cy5}Ub-His-^{Cy3}Ub [16]. Ub-His or ^{Cy5}Ub-His was mixed with a limited amount of ^{Cy3}Ub in the presence of the ubiquitination machinery in reaction buffer (50 mM HEPES-KOH, pH 7.6, 150 mM KCl, 5 mM $MgCl_2$, 0.5 mM DTT and 10 mM ATP) at final concentrations of 1.5 μM Ube1, 25 μM gp78RING-Ube2g2, 250 μM Ub-His or ^{Cy5}Ub-His, and 50 μM ^{Cy3}Ub. Reactions were incubated at 37°C for 40 min before loading them onto Ni-NTA resin equilibrated with NiA buffer. Proteins were eluted with NiB buffer, concentrated, and subjected to size-exclusion chromatography (Superdex 75 increase 10/300) in GF buffer. Peak fractions were analyzed by SDS-PAGE, and fractions containing di-Ub were pooled and concentrated. Ub-His-^{Cy3}Ub or ^{Cy5}Ub-His-^{Cy3}Ub were elongated with unlabeled ubiquitin in the presence of ubiquitination machinery at 37°C for 2.5 h. Final concentrations were 7.5 μM Ube1, 125 μM gp78RING-Ube2g2, 100 μM Ub-His-^{Cy3}Ub or ^{Cy5}Ub-His-^{Cy3}Ub, and 1 M ubiquitin, with ubiquitin being added in 200 mM aliquots every 30 min. Ubiquitin chains were purified by Ni-NTA affinity and size-exclusion chromatography (Superdex 200 increase 10/300). Fractions with chains containing more than 8 Ub moieties were pooled and concentrated.

Single-turnover unfolding assays

Single-turnover unfolding assays for ubiquitinated Eos or the Eos-Turquoise fusion substrate were performed using a BMG Labtech CLARIOstar plate reader at 37°C. Substrate was preincubated with ATP regeneration mix (see below), and p97 was incubated with cofactor(s) in assay buffer (50 mM HEPES-KOH, 150 mM KCl, 5 mM $MgCl_2$, 1 mM DTT). The reaction was initiated by mixing the substrate with p97/cofactors in 1:1 volume ratio. The final concentrations were 20 nM substrate, 400 nM p97, 2 μM UN and/or 2 μM Faf, and 1X ATP regeneration mix (5 mM ATP, 0.03 mg/mL creatine kinase, 16 mM creatine phosphate). Unfolding was monitored by measuring the loss of fluorescence, at 585 nm after excitation at 565 nm for red Eos, at 520 nm after excitation at 500 nm for green Eos, and at 475 nm after excitation at 415 nm for Turquoise. Fluorescence traces were fitted by single-exponential decay functions using GraphPad Prism.

Complex assembly and cryo-EM sample preparation

p97 was pre-incubated with UN, Faf1, and Eos substrate carrying ubiquitin chains with ~ 8 Ub moieties at 37°C for 10 min, before addition of 2 mM ATP and 10 more minutes of incubation. The final concentrations were 10 μM p97, 20 μM UN, and 20 μM Faf1. The mixture was subjected to size-exclusion chromatography (Superose 6 increase 10/300) in GF buffer supplemented with 2 mM ATPγS. Peak fractions were concentrated, concentrations were determined with BCA assays, and samples were snap frozen. For grid preparation, 3 μL of 4 mg/mL assembled complex was applied to an UltrAuFoil grid (r1.2/1.3, 300 mesh) that was glow-discharged using PELCO easiGlow system (25 mA, 25 s), and grids were plunge-frozen in liquid ethane using a Vitrobot Mark IV (Thermo Fisher Scientific) set to 4°C and 100% humidity with 4 s blot time.

Cryo-EM data collection, single-particle analysis and model building

Grids were screened on a 200 kV Talos Arctica microscope (Cal Cryo Facility at UC Berkeley) and data collection was performed at the HHMI Janelia Research Campus, using SerialEM[44] on a 300 kV Titan Krios G4 equipped with SelectrisX energy filter (6eV slit width) and a Falcon4i camera at a nominal magnification of ×165,000, corresponding to a pixel size of 0.743 Å. A dataset of 24,016 movies was recorded with a total dose of 50 $e^-/Å^2$ and a defocus range of -0.8 to -1.6 μm. Detailed data processing steps are shown in Fig. S2. Multi-frame movies were imported into cryoSPARC Live for motion correction and CTF estimation, and downstream steps were carried out using cryoSPARC v4.6 [45,46]. Particles picked with Blob picker were subjected to 2D classification and ab-initio reconstruction to get rid of junk particles. A subset of the particle stack was used as seeds for Topaz training, and the trained model was used to extract particles out of the whole dataset[47,48]. After extraction, the particles were subjected to 2D classification, ab-initio reconstruction, and heterogeneous refinement. The main class with p97 NTD in the “up” conformation was further refined with C6 symmetry, and the density of five p97 subunits was subtracted after symmetry expansion to leave out a single subunit for focused 3D classification and local refinement of the p97-NTD/Faf1-UBX region. For model building, an Alphafold3-predicted structural model was docked into the local map, manually adjusted using ISOLDE[49] in ChimeraX[50], COOT[51], and finally refined using PHENIX

real space refinement[52].

ATPase assays

The rate of ATP hydrolysis was measured using a coupled assay that monitors the decrease in NADH absorbance[53] in a plate reader at 37°C. p97/cofactors and the substrate/ATPase mix (5 mM ATP, 1 mM NADH, 7.5 mM phosphoenolpyruvate, 12 U/mL pyruvate kinase, 18 U/mL lactate dehydrogenase) were pre-incubated separately and mixed in 1:1 volume ratio right before the measurement. The absorbance of NADH at 340 nm was monitored, and ATPase rates were determined by linear regression. The final concentrations were 50 nM p97, 250 nM UN, 250 nM Faf variant, and 250 nM ubiquitinated Eos substrate.

FRET-based pore-insertion and initiator-unfolding assays

Steady-state FRET assays were performed using a BMG Labtech CLARIOstar plate reader at 37°C. p97 was pre-incubated with UN/Faf1 in assay buffer, and labeled polyubiquitin chains were incubated separately in assay buffer supplemented with ATP or ATPγS for 10 min. p97/UN/Faf1 was mixed with substrate in a 1:1 volume ratio and transferred to a 384-well plate. The plate was incubated in the plate reader at 37°C for 1 min before scanning the fluorescence emission from 550 nm to 750 nm after excitation at 480 nm. The final concentrations were 200 nM ^{LD655}p97, 2 μM UN, 2 μM Faf variant, and 200 nM Ub-^{Cy3}Ub-Ub$_n$ for pore insertion assays. For the initiator-unfolding assay, final concentrations were 2 μM p97, 2 μM UN, 2 μM Faf variant, and 200 nM ^{Cy5}Ub-^{Cy3}Ub-Ub$_n$. The fluorescence intensities for each spectrum were normalized relative to the Cy3 emission maximum at 568 nm.

The kinetics of initiator insertion into p97 were measured in an Auto SF120 stopped-flow fluorometer (Kintek). The syringes were loaded with 145 μL of ^{LD655}p97/UN/Faf1 and substrates/ATP, respectively, and incubated at 37°C. After loading, 7 shots of 35 μL each were fired, and the last three were analyzed. The final concentrations were 1 μM ^{LD655}p97/UN/Faf1 and 0.1 μM Ub-^{Cy3}Ub-Ub$_n$ chains. An excitation wavelength of 480 nm was used, and the fluorescence of donor and acceptor dyes were measured simultaneously in different channels.

Figures

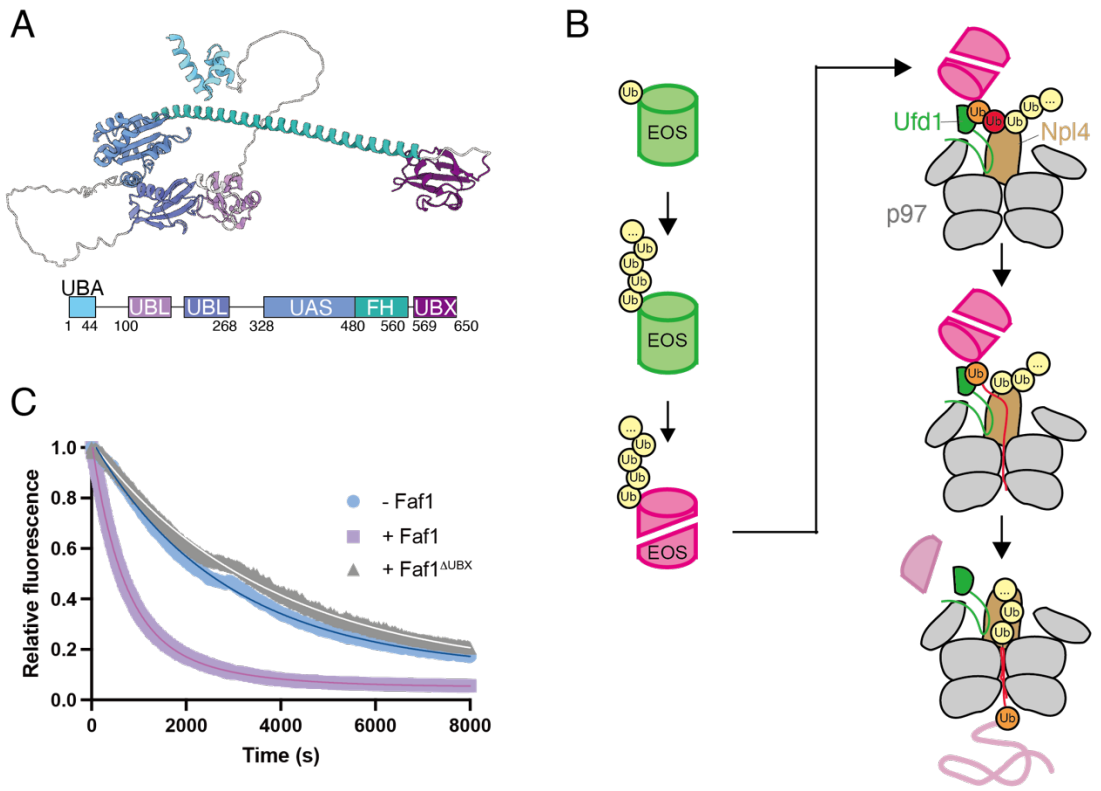

Figure 1. Faf1 accelerates the unfolding of ubiquitinated substrates. A) Top: Alphafold3 predicted structure of human Faf1, colored by domains. Bottom: Schematic of Faf1 domain architecture. **B)** Left: Overview of substrate preparation. mEos3.2 fused to mono-ubiquitin was poly-ubiquitinated and photoconverted by UV irradiation to red Eos with cleaved backbone. Right: The substrate-unfolding assay monitors the loss of red Eos fluorescence, after an initiator ubiquitin (red sphere) was bound and unfolded by Npl4 (tan), which is facilitated by the interaction of the proximally neighboring ubiquitin (orange sphere) with the UT3 domain of Ufd1, followed by unfolding and threading of the entire proximal part of the chain as well as the Eos substrate. Ubiquitin moieties located on the distal side of the initiator (light yellow spheres) do not get unfolded by p97. **C)** Traces for the loss of red Eos fluorescence upon unfolding by p97-UN in the absence and presence of Faf1. All traces represent the averages of three independent measurements that were normalized to the starting fluorescence value. Solid lines show the single-exponential fits.

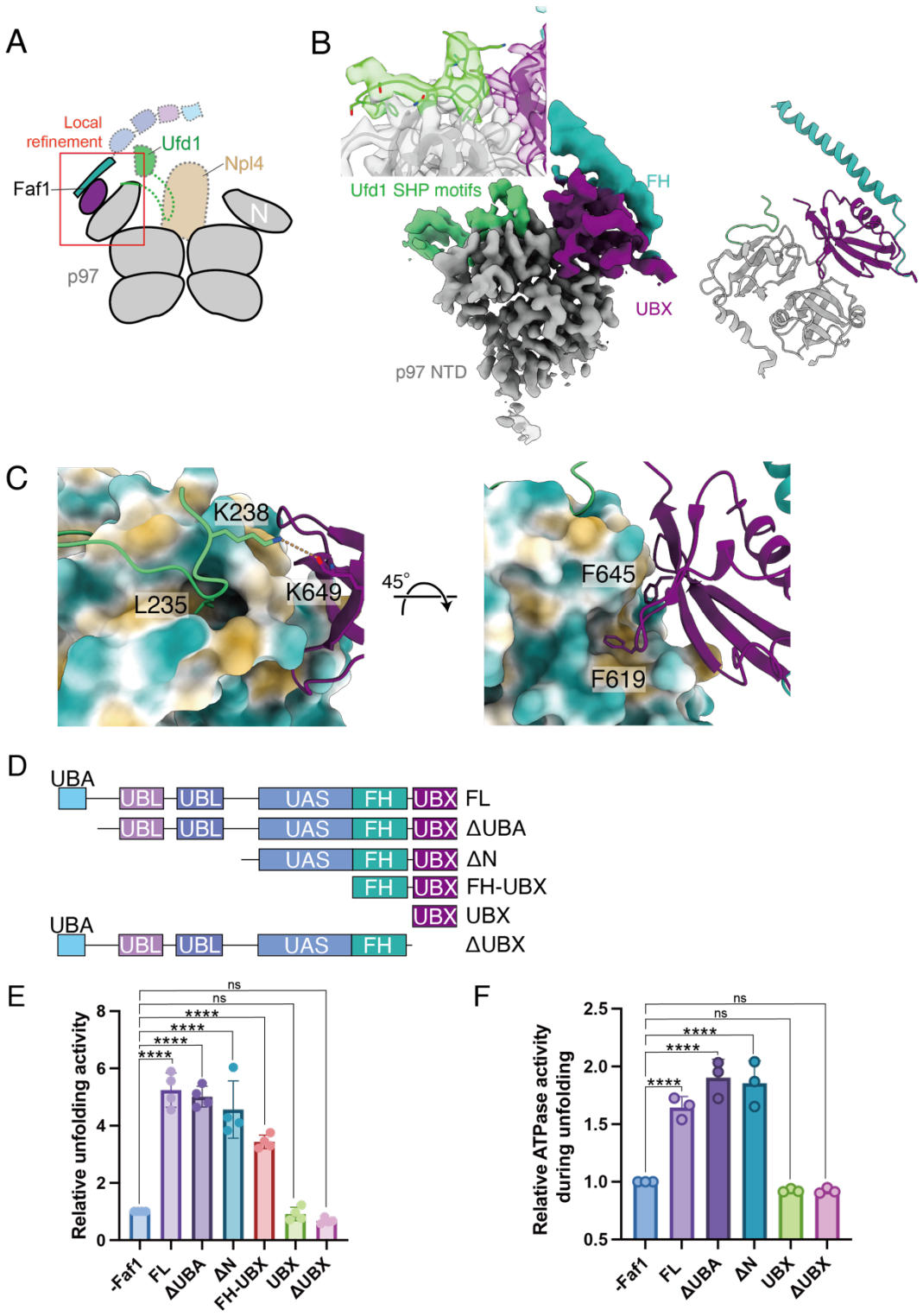

Figure 2. Structural and biochemical analyses of the p97-UN-Faf1 complex. A) Schematic of the p97-UN-Faf1 complex, with parts not resolved in our cryo-EM structure shown faded and with dashed outlines. The red box indicates the area for focused classification and local refinement in our single-particle analysis. **B)** Cryo-EM density (left) and atomic model (right) of the complex between p97 NTD (grey), Faf1's helix (FH, turquoise) and

UBX domain (purple), and Ufd1's SHP motif (green). A focused view of the transparent map and atomic model of the SHP-interacting region is shown on the top left. **C)** Close-up view of interactions between p97 NTD (represented as surface and colored by hydrophobicity), Ufd1's SHP motif (green), and Faf1's UBX domain (purple). **D)** Schematics of Faf1 truncation mutants used in biochemical experiments. **E)** Relative substrate-unfolding activities of p97-UN in the absence of Faf1 (normalized to 1) and in the presence of saturating full-length or truncated Faf1. Shown are the mean values and standard deviations for the mean for four technical replicates. Statistical significance was calculated using a one-way ANOVA test: ****$p<0.0001$; ns, $p>0.05$. **F)** Relative ATPase activities of p97-UN during unfolding of ubiquitinated green Eos in the absence of Faf1 (normalized to 1) and the presence of full-length or truncated Faf1. Shown are the mean values and standard deviations for the mean for three technical replicates. Statistical significance was calculated using a one-way ANOVA test: ****$p<0.0001$; ns, $p>0.05$.

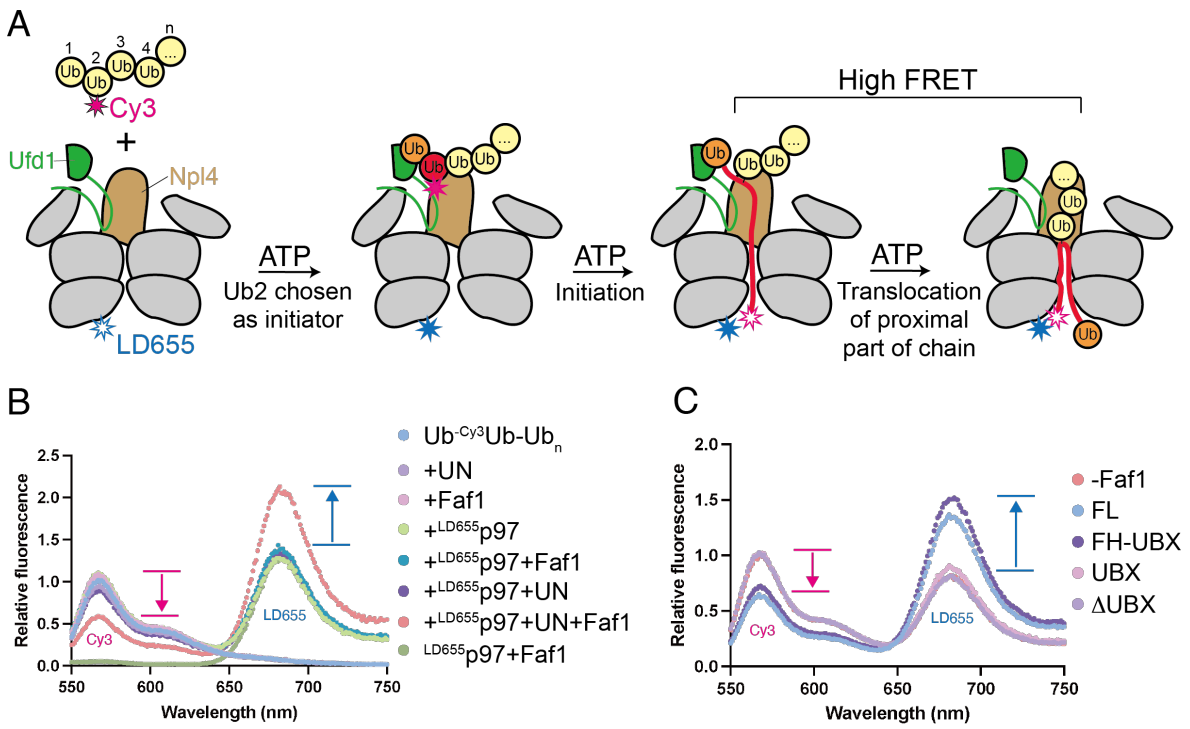

Figure 3. FRET-based unfolding-initiation assay. A) Experimental design for the initiation assay, with unanchored poly-ubiquitin chains (> 10 moieties) labeled with Cy3 (red star) on the N-terminus of the second ubiquitin and p97 labeled with LD655 (blue star) near the exit of the processing channel. UN choosing ubiquitin 2 as the initiator (top) leads to an immediate FRET-signal change that persists when p97 stalls on the proximal part of the ubiquitin chain. **B)** Normalized fluorescence emission spectra after excitation at 480 nm for ubiquitin chains with Cy3 attached to ubiquitin 2 (Ub-^{Cy3}Ub-Ub$_n$) in the absence and presence of LD655-labeled p97 (^{LD655}p97), UN, and Faf1, or for ^{LD655}p97 with Faf1 alone. Arrows indicate the changes in Cy3- and LD655-fluorescence intensities upon unfolding initiation. **C)** Normalized fluorescence emission spectra after Cy3 excitation for samples with Ub-^{Cy3}Ub-Ub$_n$, ^{LD655}p97, and UN in the absence or presence of different Faf1 truncation mutants. Arrows indicate the changes in Cy3- and LD655-fluorescence intensities upon unfolding initiation.

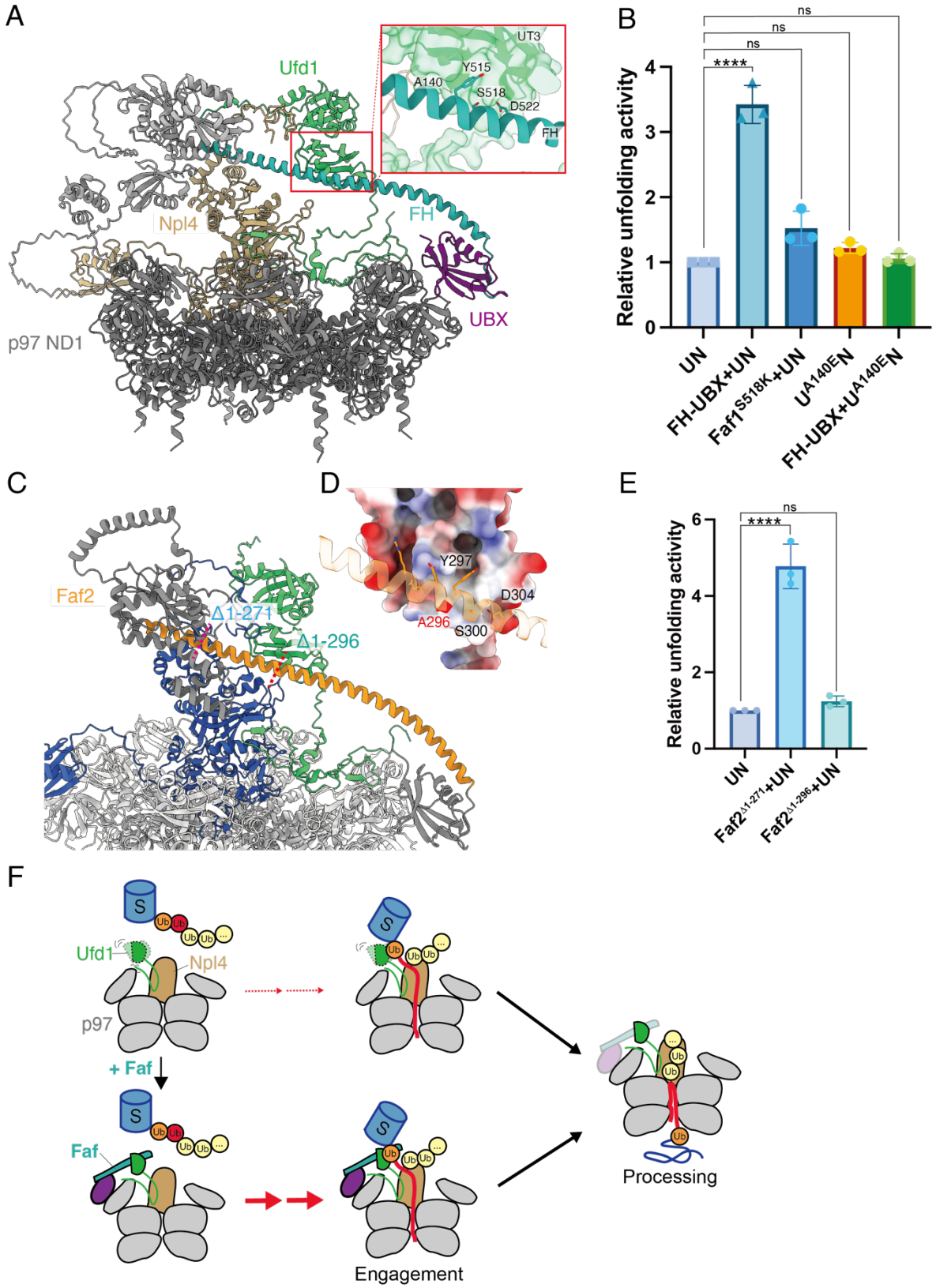

Figure 4. Faf1's C-terminal helix facilitates initiator-ubiquitin unfolding and insertion into p97. A) AlphaFold3 model for the complex between p97's N-terminal and D1 ATPase domains (ND1, dark grey), Npl4 (tan), Ufd1 (green), and Faf1, with Faf1's UBA, UBL, and UAS

domain depicted in light grey, the long helix (FH) in turquoise, and the UBX domain in purple. The red box shows a zoom-in of the interface between Faf1's long helix and Ufd1's UT3 domain. **B)** Relative mEos-substrate unfolding activities for p97 in the presence of wild-type UN, wild-type Faf1 FH-UBX fragment, UN with Ufd1 carrying an A140E mutation in its UT3 domain at the FH-binding interface, or Faf1 with a S518K mutation in its predicted UT3-binding interface. Shown are the mean values and standard deviations for the mean for three technical replicates. Statistical significance was calculated using a one-way ANOVA test: ****$p<0.0001$; ns, $p>0.05$. **C)** AlphaFold3 model for the complex between p97's ND1 portion (light grey), Npl4 (dark blue), Ufd1 (green), and Faf2, with the long helix shown on orange and the rest of Faf2 in dark grey. Positions for Faf2 N-terminal truncation mutants Δ1-271 and Δ1-296 are indicated by red dashed lines. **D)** Close-up view of the interface between Ufd1's UT3 domain and Faf2's FH helix, with UT3 shown in surface representation and colored by electrostatic properties. **E)** Relative mEos-substrate unfolding activities for p97-UN in the absence or presence of Faf2 N-terminal truncation variants. Shown are the mean values and standard deviations for the mean for three technical replicates. Statistical significance was calculated using a one-way ANOVA test: ****$p<0.0001$; ns, $p>0.05$. **F)** Model for Faf-mediated engagement and unfolding of a ubiquitinated substrate (blue) by p97-UN. In the absence of a Faf cofactor, Ufd1's UT3 domain may have higher flexibility that hampers the binding, unfolding, and motor engagement of the initiator ubiquitin (red sphere). Faf binding stabilizes the UT3 domain through its long helix (turquoise) that is anchored on its p97 NTD-bound UBX domain (purple), facilitating unfolding initiation and overall substrate processing.

Supplemental Figures

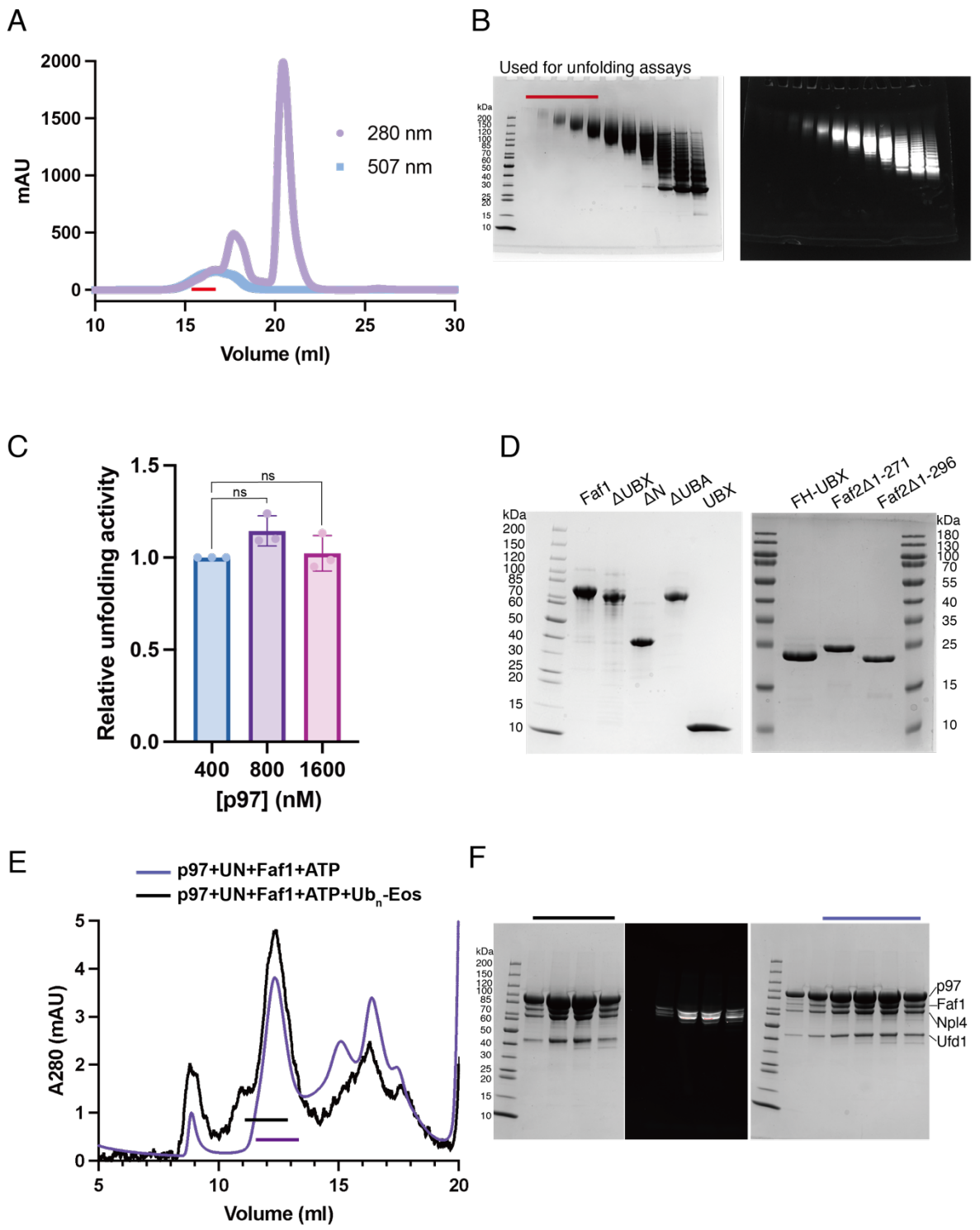

Supplemental Figure S1. Sample preparations for biochemical and cryo-EM experiments. A) Size-exclusion chromatogram for the purification of poly-ubiquitinated mEos substrate, monitored by general protein absorbance at 280 nm (purple) and mEos absorbance at 507 nm (light blue). Fractions pooled and used for unfolding experiments are indicated by

a red bar. **B)** SDS-PAGE gels with the peak fractions of the size-exclusion chromatography shown in (A) and visualized by Coomassie staining (left) or mEos fluorescence (right). Fractions pooled and used for unfolding experiments are indicated by a red bar. **C)** Confirmation of single-turnover conditions for substrate unfolding. The rates for unfolding of the Eos substrate (20 nM) in the presence of UN (2 μM) and Faf1 (2 μM) did not significantly change when the p97 concentration was increased from 400 nM to 1600 nM, confirming saturating conditions for single-turnover kinetics. Shown are the mean values of the relative rates and the standard deviation of the mean for 3 technical replicates. Shown are the mean values and standard deviations for the mean for three technical replicates. Statistical significance was calculated using a one-way ANOVA test: ns, $p>0.05$. **D)** Coomassie-stained SDS-PAGE gels of purified full-length and truncated variants of Faf1 (left) and Faf2 (right). **E)** Size-exclusion chromatogram for the purification of the p97-UN-Faf1 complex with ATP in the absence (purple) or presence (black) of poly-ubiquitinated (5-7 moieties) mEos substrate. Horizontal bars indicate fractions that were pooled and used for cryo-EM. **F)** SDS-PAGE gels with the peak fractions of the size-exclusion purifications shown in (E), visualized by Coomassie-staining (left) and mEos fluorescence (middle) for the substrate-containing sample, and visualized by Coomassie-staining for the substrate-free sample (right). Black and purple bars indicate the fractions that contained all components, were pooled, and used for cryo-EM sample preparations.

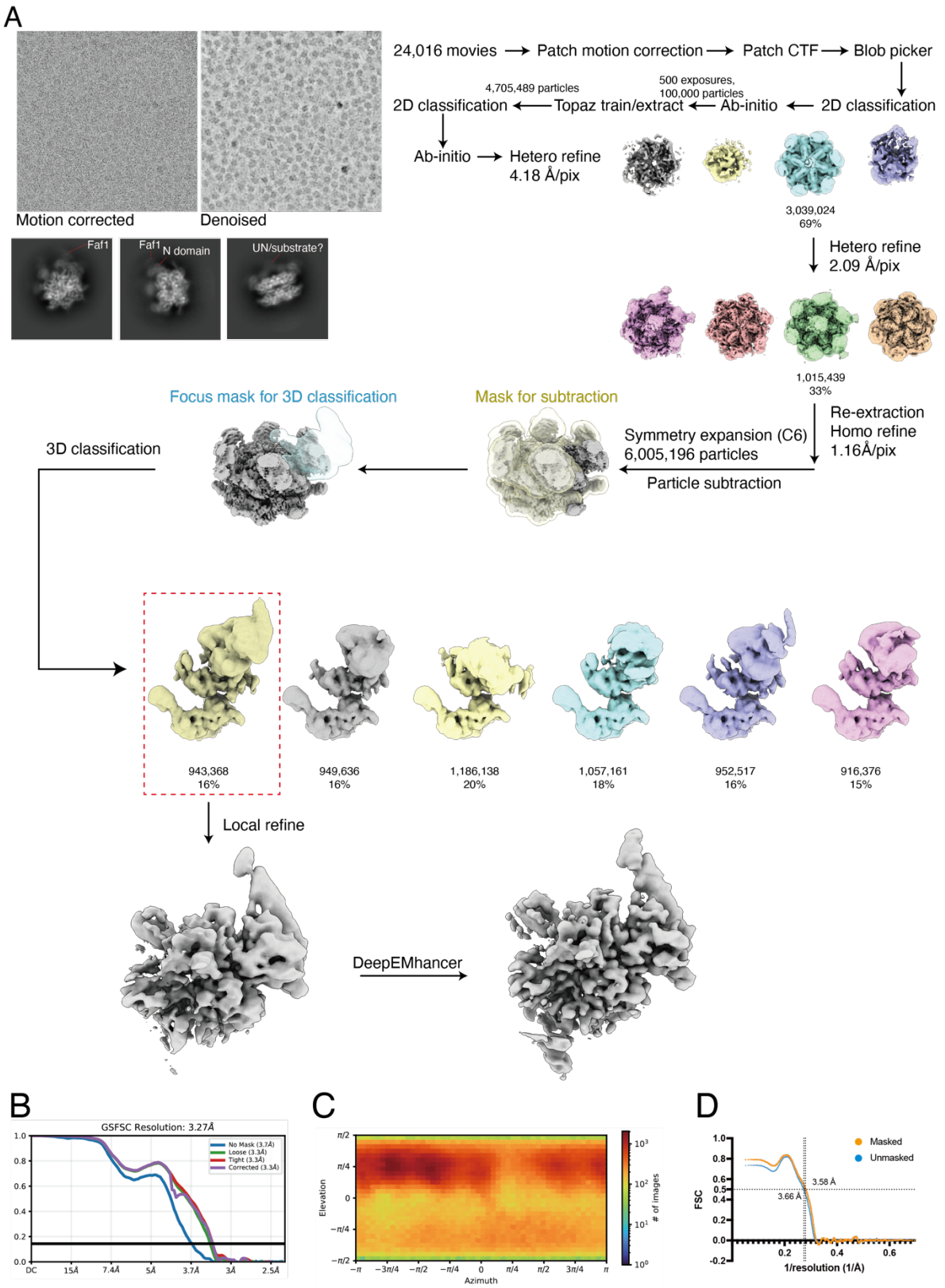

Supplemental Figure S2. Cryo-EM single-particle analysis of the p97-UN-Faf1-substrate complex. A) Data-processing workflow using CryoSPARC. **B)** GSFSC curve and **C)** orientation distribution of the final map. **D)** Map-model FSC curve calculated after the final refinement in PHENIX.

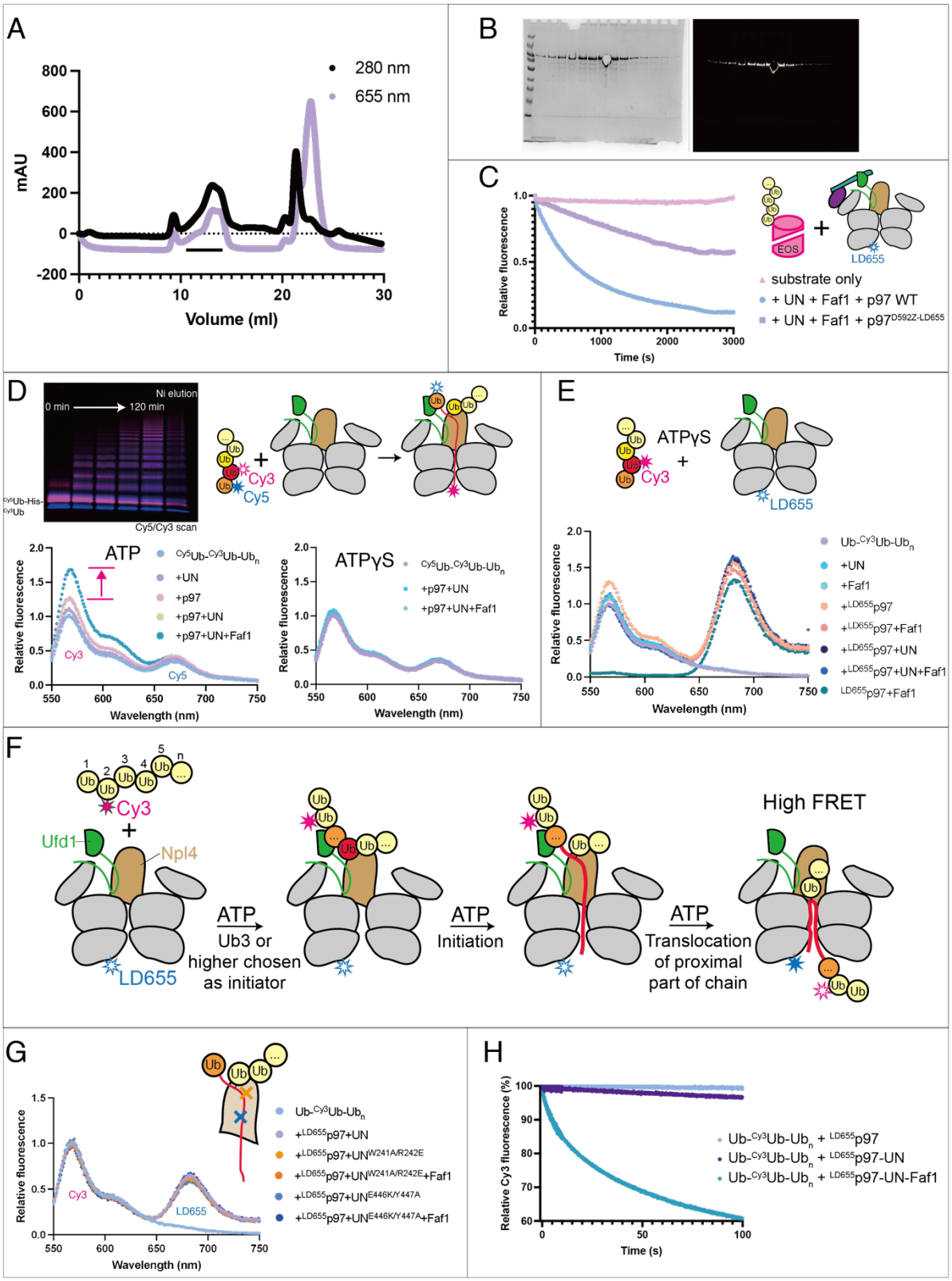

Supplemental Figure S3. Extended results for FRET-based ubiquitin unfolding and initiation assays. A) Size -exclusion chromatogram for the purification of LD655-labeled p97^{D592AzF}, detected by protein absorbance at 280 nm (black) or LD655 absorbance at 655 nm (purple). **B)** SDS-PAGE gels with the peak fractions of the purification show in (A) and

visualized by Coomassie stain (left) or LD655-fluorescence scan (right). **C)** Example traces for the mEos-substrate unfolding by wild-type p97 or LD655-labeled p97, both in the presence of UN and Faf1 cofactors. **D)** Initiator-ubiquitin unfolding measured by the loss of FRET between Cy5 attached to the first ubiquitin and Cy3 attached to the second ubiquitin in unanchored ubiquitin chains (^{Cy5}Ub-^{Cy3}Ub-Ub$_n$) after incubation with p97, UN, and Faf1. The gel image on the top left shows an overlay of Cy3- and Cy5-fluorescence scans for the SDS-PAGE analysis of doubly labeled ^{Cy5}Ub-^{Cy3}Ub-Ub$_n$ synthesis progression over 120 min and the final sample after Ni-NTA affinity purification. Shown at the bottom are the normalized fluorescence emission spectra after excitation at 480 nm for the samples incubated with ATP (left) or ATPγS (right). **E)** FRET-based unfolding initiation assay with unanchored Ub-^{Cy3}Ub-Ub$_n$ ubiquitin chains, ^{LD655}p97, UN, and Faf1 as shown in Fig. 3, but using ATPγS instead of ATP. Shown are normalized example spectra for the fluorescence emission after excitation at 480 nm. **F)** FRET-based initiation assay with unanchored Ub-^{Cy3}Ub-Ub$_n$ ubiquitin chains and ^{LD655}p97 as shown in Fig.3A, but assuming that UN chooses ubiquitin 3 or higher in the chain, such that ATP-dependent unfolding and translocation of the proximally located ubiquitins is required to move the Cy3-labeled second ubiquitin into proximity of LD655 for a FRET-signal change. **G)** Same FRET-based initiation assay, but using Npl4 variants carrying W241A/R242E (orange) or E446K/Y447A double mutations (blue) in the hydrophobic groove that prevent binding and unfolding of the initiator ubiquitin. Shown are the normalized fluorescence emission spectra after Cy3 excitation at 480 nm. **H)** Effects of Faf1 on the kinetics of unfolding initiation by p97-UN. Shown are example traces for the Cy3-fluorescence quenching after stopped-flow mixing of unanchored Ub-^{Cy3}Ub-Ub$_n$ ubiquitin chains with ^{LD655}p97-UN in the absence or presence of Faf1.

A

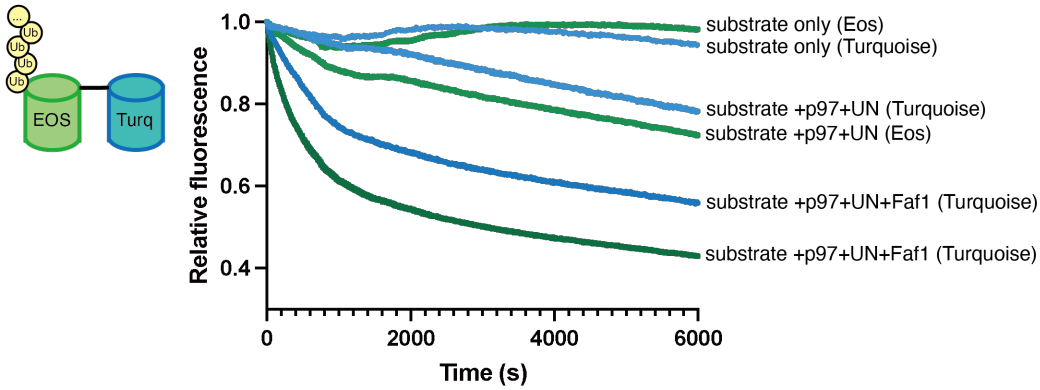

B

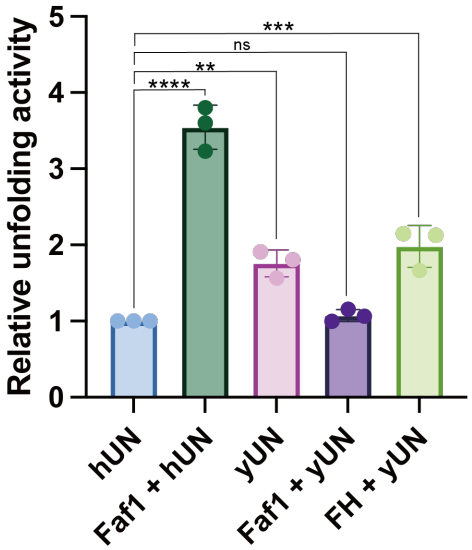

Supplemental Figure S4. A) Schematic of the poly-ubiquitinated mEos-Turquoise fusion substrate (left) and kinetics for its unfolding by p97-UN in the absence and presence of Faf1 (right). Shown are example traces for the changes in green Eos fluorescence (shades of green) and changes in Turquoise fluorescence (shades of blue) that were measured separately after mixing the fusion substrate with p97 and cofactors. Loss in Turquoise fluorescence indicates that the Eos moiety of the substrate was completely unfolded and translocated. **B)** Relative rates for the unfolding of poly-ubiquitinated mEos substrate by p97 in the presence of human UN (hUN), yeast UN (yUN), and full-length Faf1 or the FH-UBX fragment. Shown are the mean values and standard deviations of the mean for three technical replicates. Statistical significance was calculated using a one-way ANOVA test: ****p<0.0001; ***p<0.001;**p<0.01;

ns, $p>0.05$. The Eos substrate for these series of measurements carried slightly shorter ubiquitin chains (< 8 moieties) than the substrate for the measurements in Fig. 2E (8-12 ubiquitin moieties).

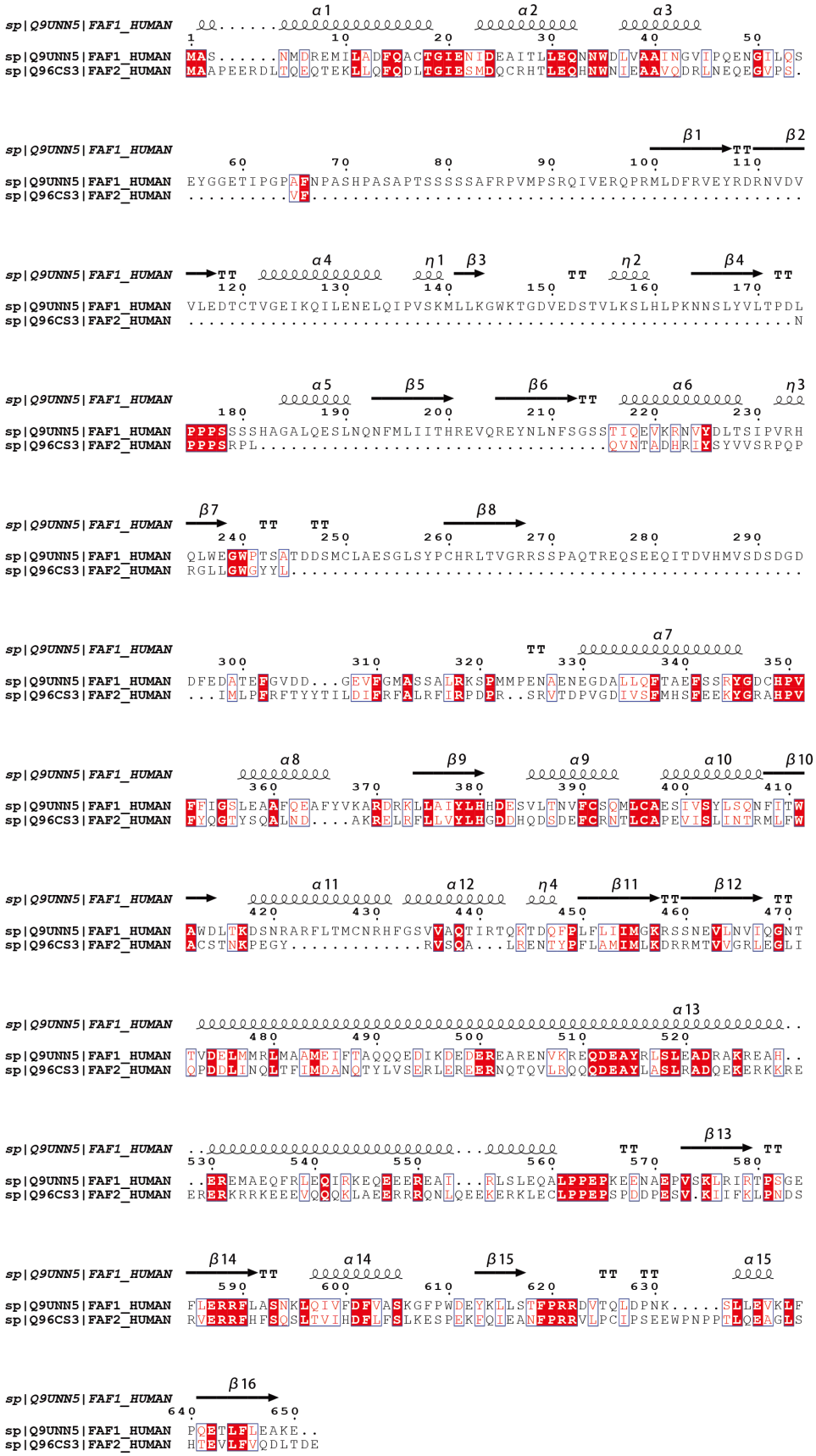

Supplemental Figure S5. Sequence alignment of human Faf1 and Faf2.

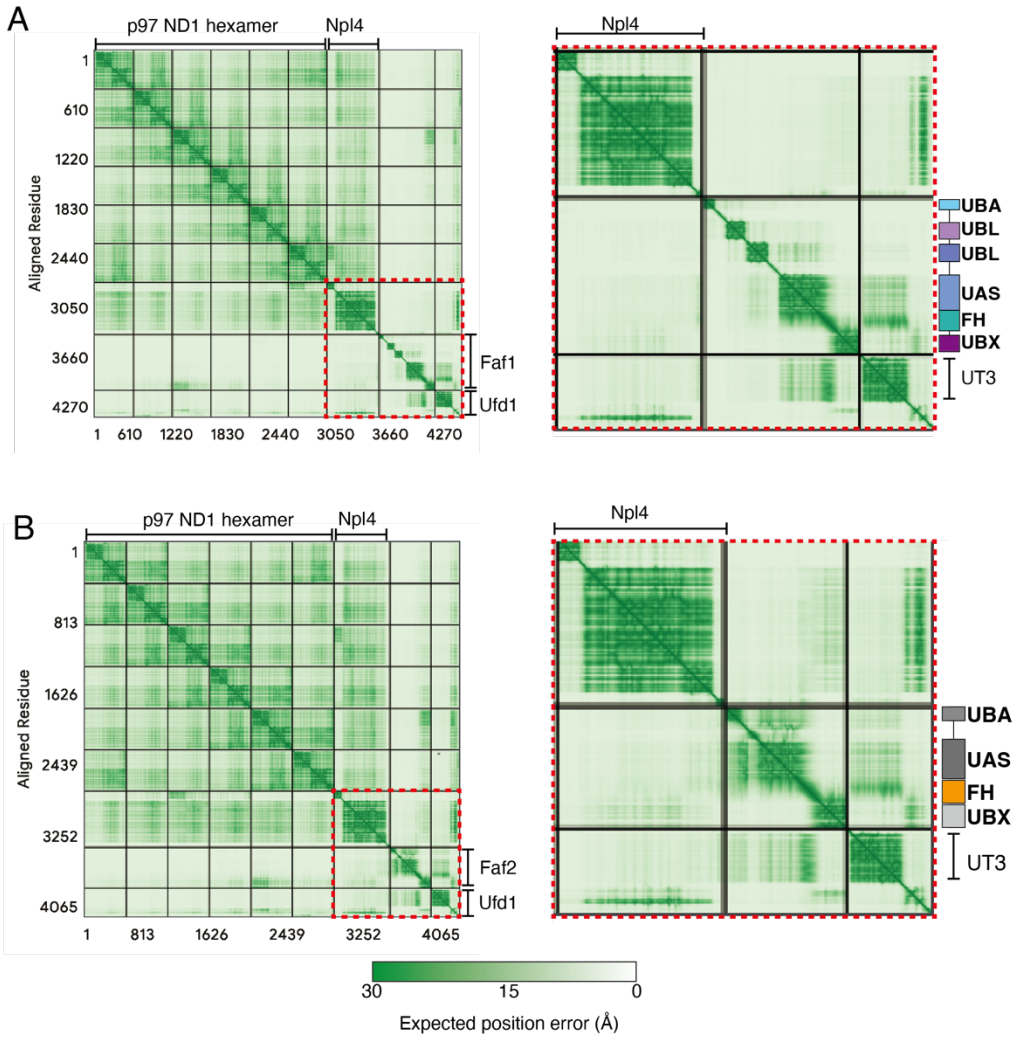

Supplemental Figure S6. Predicted align error (PAE) for the Alphafold3 models of the p97-UN-Faf complexes. A) Left: PAE plot for the entire input of p97 NTD-D1, UN, and Faf1. Right: Zoom-in view of the Faf1-UN interaction, as highlighted by the red dashed box on the left. **B)** Left: PAE plot for the entire input of p97 NTD-D1, UN, and the Faf2 UBA-UAS-FH-UBX fragment. Right: Zoom-in view of the Faf2-UN interaction, as highlighted by the red dashed box on the left.

	p97-Ufd1-Faf1 complex structure (NTD focused)
EMDB entry	73536
PDB entry	9YW2
Data collection and processing	
Microscope and camera	Titan Krios G4, Falcon 4i
Magnification	×165,000
Voltage (kV)	300
Data acquisition software	SerialEM
Electron exposure (e^-/Å)	50
Defocus range (μM)	-0.8 to -1.6
Pixel size (Å)	0.743
Symmetry imposed	C1
Initial particle images (no.)	4,705,489
Final particle images (no.)	943,368
Map resolution (Å)	3.27
FSC threshold	0.143
Refinement	
Initial model	Alphafold3
Model resolution (Å)	3.58
FSC threshold	0.5
Map sharpening *B* factor (Å^2)	143.9
Model compositions	
Non-hydrogen atoms	2610
Protein residues	323
Ligands	0
***B* factors (Å^2)**	
Protein	158.39
Ligand	N/A
R.m.s. deviations	
Bond lengths (Å)	0.003
Bond angles (°)	0.761
Validation	
MolProbity score	2.43
Clashscore	16.99
Poor rotamoers (%)	3.09
Ramachandran plot	
Favored (%)	95.27
Allowed (%)	4.10
Disalowed (%)	0.63

Table 1: Cryo-EM data collection, refinement and validation statistics, and atomic model for the p97-Ufd1-Faf1 complex.

References:

1. Stein, A., Ruggiano, A., Carvalho, P., and Rapoport, T.A. (2014). Key steps in ERAD of luminal ER proteins reconstituted with purified components. Cell *158*, 1375-1388. 10.1016/j.cell.2014.07.050.
2. Brodsky, J.L. (2012). The interaction of factors required for ER associated degradation (ERAD). Faseb Journal *26*.
3. Wolf, D.H., and Stolz, A. (2012). The Cdc48 machine in endoplasmic reticulum associated protein degradation. Biochim Biophys Acta *1823*, 117-124. 10.1016/j.bbamcr.2011.09.002.
4. Moreno, S.P., Bailey, R., Campion, N., Herron, S., and Gambus, A. (2014). Polyubiquitylation drives replisome disassembly at the termination of DNA replication. Science *346*, 477-481. 10.1126/science.1253585.
5. Maric, M., Maculins, T., De Piccoli, G., and Labib, K. (2014). Cdc48 and a ubiquitin ligase drive disassembly of the CMG helicase at the end of DNA replication. Science *346*, 1253596. 10.1126/science.1253596.
6. van den Boom, J., Wolf, M., Weimann, L., Schulze, N., Li, F.H., Kaschani, F., Riemer, A., Zierhut, C., Kaiser, M., Iliakis, G., et al. (2016). VCP/p97 Extracts Sterically Trapped Ku70/80 Rings from DNA in Double-Strand Break Repair. Molecular Cell *64*, 189-198. 10.1016/j.molcel.2016.08.037.
7. van den Boom, J., and Meyer, H. (2018). VCP/p97-Mediated Unfolding as a Principle in Protein Homeostasis and Signaling. Mol Cell *69*, 182-194. 10.1016/j.molcel.2017.10.028.
8. Watts, G.D., Wymer, J., Kovach, M.J., Mehta, S.G., Mumm, S., Darvish, D., Pestronk, A., Whyte, M.P., and Kimonis, V.E. (2004). Inclusion body myopathy associated with Paget disease of bone and frontotemporal dementia is caused by mutant valosin-containing protein. Nat Genet *36*, 377-381. 10.1038/ng1332.
9. Nalbandian, A., Donkervoort, S., Dec, E., Badadani, M., Katheria, V., Rana, P., Nguyen, C., Mukherjee, J., Caiozzo, V., Martin, B., et al. (2011). The multiple faces of valosin-containing protein-associated diseases: inclusion body myopathy with Paget's disease of bone, frontotemporal dementia, and amyotrophic lateral sclerosis. J Mol Neurosci *45*, 522-531. 10.1007/s12031-011-9627-y.
10. Al-Obeidi, E., Al-Tahan, S., Surampalli, A., Goyal, N., Wang, A.K., Hermann, A., Omizo, M., Smith, C., Mozaffar, T., and Kimonis, V. (2018). Genotype-phenotype study in patients with valosin-containing protein mutations associated with multisystem proteinopathy. Clinical Genetics *93*, 119-125. 10.1111/cge.13095.
11. DeLaBarre, B., and Brunger, A.T. (2003). Complete structure of p97/valosin-containing protein reveals communication between nucleotide domains. Nature Structural Biology *10*, 856-863. 10.1038/nsb972.
12. Twomey, E.C., Ji, Z., Wales, T.E., Bodnar, N.O., Ficarro, S.B., Marto, J.A., Engen, J.R., and Rapoport, T.A. (2019). Substrate processing by the Cdc48 ATPase complex is initiated by ubiquitin unfolding. Science *365*. 10.1126/science.aax1033.
13. Tsuchiya, H., Ohtake, F., Arai, N., Kaiho, A., Yasuda, S., Tanaka, K., and Saeki, Y. (2017). In Vivo Ubiquitin Linkage-type Analysis Reveals that the Cdc48-Rad23/Dsk2 Axis Contributes to K48-Linked Chain Specificity of the Proteasome. Molecular Cell *66*,

488-502.e487. 10.1016/j.molcel.2017.04.024.
14. Williams, C., Dong, K.C., Arkinson, C., and Martin, A. (2023). The Ufd1 cofactor determines the linkage specificity of polyubiquitin chain engagement by the AAA+ ATPase Cdc48. Mol Cell *83*, 759-769 e757. 10.1016/j.molcel.2023.01.016.
15. Lee, H.G., Lemmon, A.A., and Lima, C.D. (2023). SUMO enhances unfolding of SUMO-polyubiquitin-modified substrates by the Ufd1/Npl4/Cdc48 complex. Proc. Natl. Acad. Sci. U.S.A. *120*. ARTN e2213703120
10.1073/pnas.2213703120.
16. Williams, C., Dong, K.C., Arkinson, C., and Martin, A. (2023). Preparation of site-specifically fluorophore-labeled polyubiquitin chains for FRET studies of Cdc48 substrate processing. STAR Protoc *4*, 102659. 10.1016/j.xpro.2023.102659.
17. Ji, Z., Li, H., Peterle, D., Paulo, J.A., Ficarro, S.B., Wales, T.E., Marto, J.A., Gygi, S.P., Engen, J.R., and Rapoport, T.A. (2022). Translocation of polyubiquitinated protein substrates by the hexameric Cdc48 ATPase. Mol Cell *82*, 570-584 e578. 10.1016/j.molcel.2021.11.033.
18. Blythe, E.E., Gates, S.N., Deshaies, R.J., and Martin, A. (2019). Multisystem Proteinopathy Mutations in VCP/p97 Increase NPLOC4.UFD1L Binding and Substrate Processing. Structure *27*, 1820-1829 e1824. 10.1016/j.str.2019.09.011.
19. Fujisawa, R., Polo Rivera, C., and Labib, K.P.M. (2022). Multiple UBX proteins reduce the ubiquitin threshold of the mammalian p97-UFD1-NPL4 unfoldase. eLife *11*. 10.7554/eLife.76763.
20. Blythe, E.E., Olson, K.C., Chau, V., and Deshaies, R.J. (2017). Ubiquitin- and ATP-dependent unfoldase activity of P97/VCP*NPLOC4*UFD1L is enhanced by a mutation that causes multisystem proteinopathy. Proc Natl Acad Sci U S A *114*, E4380-E4388. 10.1073/pnas.1706205114.
21. Kochenova, O.V., Mukkavalli, S., Raman, M., and Walter, J.C. (2022). Cooperative assembly of p97 complexes involved in replication termination. Nature communications *13*, 6591. 10.1038/s41467-022-34210-y.
22. Song, S., Lee, J.J., Kim, H.J., Lee, J.Y., Chang, J., and Lee, K.J. (2016). Fas-Associated Factor 1 Negatively Regulates the Antiviral Immune Response by Inhibiting Translocation of Interferon Regulatory Factor 3 to the Nucleus. Molecular and cellular biology *36*, 1136-1151. 10.1128/Mcb.00744-15.
23. Dai, T., Wu, L.M., Wang, S., Wang, J., Xie, F., Zhang, Z.K., Fang, X.W., Li, J.X., Fang, P.F., Li, F., et al. (2018). FAF1 Regulates Antiviral Immunity by Inhibiting MAVS but Is Antagonized by Phosphorylation upon Viral Infection. Cell Host Microbe *24*, 776-+. 10.1016/j.chom.2018.10.006.
24. Körner, M., Müller, P., Das, H., Kraus, F., Pfeuffer, T., Spielhaupter, S., Oeljeklaus, S., Schülein-Völk, C., Harper, J.W., Warscheid, B., and Buchberger, A. (2025). p97/VCP is required for piecemeal autophagy of aggresomes. Nature communications *16*. ARTN 4243
10.1038/s41467-025-59556-x.
25. Ewens, C.A., Panico, S., Kloppsteck, P., McKeown, C., Ebong, I.O., Robinson, C., Zhang, X.D., and Freemont, P.S. (2014). The p97-FAF1 Protein Complex Reveals a Common Mode of p97 Adaptor Binding. J. Biol. Chem. *289*, 12077-12084.

10.1074/jbc.M114.559591.
26. Song, J., Park, J.K., Lee, J.J., Choi, Y.S., Ryu, K.S., Kim, J.H., Kim, E., Lee, K.J., Jeon, Y.H., and Kim, E.E. (2009). Structure and interaction of ubiquitin-associated domain of human Fas-associated factor 1. Protein Sci *18*, 2265-2276. 10.1002/pro.237.
27. Song, S.H., Park, J.K., Shin, S.C., Lee, J.J., Hong, S.K., Song, I.K., Kim, B., Song, E.J., Lee, K.J., and Kim, E.E. (2022). The complex of Fas-associated factor 1 with Hsp70 stabilizes the adherens junction integrity by suppressing RhoA activation. Journal of Molecular Cell Biology *14*. ARTN mjac037
10.1093/jmcb/mjac037.
28. Schuberth, C., and Buchberger, A. (2005). Membrane-bound Ubx2 recruits Cdc48 to ubiquitin ligases and their substrates to ensure efficient ER-associated protein degradation. Nature cell biology *7*, 999-1006. 10.1038/ncb1299.
29. Neuber, O., Jarosch, E., Volkwein, C., Walter, J., and Sommer, T. (2005). Ubx2 links the Cdc48 complex to ER-associated protein degradation. Nature cell biology *7*, 993-U992. 10.1038/ncb1298.
30. Olszewski, M.M., Williams, C., Dong, K.C., and Martin, A. (2019). The Cdc48 unfoldase prepares well-folded protein substrates for degradation by the 26S proteasome. Communications Biology *2*, 29. 10.1038/s42003-019-0283-z.
31. Bodnar, N.O., and Rapoport, T.A. (2017). Molecular Mechanism of Substrate Processing by the Cdc48 ATPase Complex. Cell *169*, 722-735 e729. 10.1016/j.cell.2017.04.020.
32. Kim, K.H., Kang, W., Suh, S.W., and Yang, J.K. (2011). Crystal structure of FAF1 UBX domain in complex with p97/VCP N domain reveals a conformational change in the conserved FcisP touch-turn motif of UBX domain. Proteins-Structure Function and Bioinformatics *79*, 2583-2587. 10.1002/prot.23073.
33. Hänzelmann, P., Buchberger, A., and Schindelin, H. (2011). Hierarchical Binding of Cofactors to the AAA ATPase p97. Structure *19*, 833-843. 10.1016/j.str.2011.03.018.
34. Hanzelmann, P., and Schindelin, H. (2016). Characterization of an Additional Binding Surface on the p97 N-Terminal Domain Involved in Bipartite Cofactor Interactions. Structure *24*, 140-147. 10.1016/j.str.2015.10.027.
35. Le, L.T.M., Kang, W., Kim, J.Y., Le, O.T.T., Lee, S.Y., and Yang, J.K. (2016). Structural Details of Ufd1 Binding to p97 and Their Functional Implications in ER-Associated Degradation. Plos One *11*. ARTN e0163394
10.1371/journal.pone.0163394.
36. Schuetz, A.K., and Kay, L.E. (2016). A Dynamic molecular basis for malfunction in disease mutants of p97/VCP. eLife *5*. 10.7554/eLife.20143.
37. Pan, M., Zheng, Q.Y., Yu, Y.Y., Ai, H.S., Xie, Y., Zeng, X., Wang, C., Liu, L., and Zhao, M.L. (2021). Seesaw conformations of Npl4 in the human p97 complex and the inhibitory mechanism of a disulfiram derivative. Nature communications *12*. ARTN 121
10.1038/s41467-020-20359-x.
38. Kim, H., Zhang, H., Meng, D., Russell, G., Lee, J.N., and Ye, J. (2013). UAS domain of Ubxd8 and FAF1 polymerizes upon interaction with long-chain unsaturated fatty acids. J Lipid Res *54*, 2144-2152. 10.1194/jlr.M037218.
39. Blueggel, M., Kroening, A., Kracht, M., van den Boom, J., Dabisch, M., Goehring, A.,

Kaschani, F., Kaiser, M., Bayer, P., Meyer, H., and Beuck, C. (2023). The UBX domain in UBXD1 organizes ubiquitin binding at the C-terminus of the VCP/p97 AAA-ATPase. Nature communications *14*. ARTN 3258
10.1038/s41467-023-38604-4.
40. Cui, S.J., Simmons, G., Vale, G., Deng, Y.Q., Kim, J., Kim, H., Zhang, R.H., McDonald, J.G., and Ye, J. (2022). FAF1 blocks ferroptosis by inhibiting peroxidation of polyunsaturated fatty acids. Proc. Natl. Acad. Sci. U.S.A. *119*. ARTN e2107189119
10.1073/pnas.2107189119.
41. Martin, A., Baker, T.A., and Sauer, R.T. (2008). Protein unfolding by a AAA+ protease is dependent on ATP-hydrolysis rates and substrate energy landscapes. Nat Struct Mol Biol *15*, 139-145.
42. Bard, J.A.M., and Martin, A. (2018). Recombinant Expression, Unnatural Amino Acid Incorporation, and Site-Specific Labeling of 26S Proteasomal Subcomplexes. Methods Mol Biol *1844*, 219-236. 10.1007/978-1-4939-8706-1_15.
43. Bard, J.A.M., Bashore, C., Dong, K.C., and Martin, A. (2019). The 26S Proteasome Utilizes a Kinetic Gateway to Prioritize Substrate Degradation. Cell *177*, 286-298 e215. 10.1016/j.cell.2019.02.031.
44. Mastronade, D.N. (2003). SerialEM: A Program for Automated Tilt Series Acquisition on Tecnai Microscopes Using Prediction of Specimen Position. Microsc Microanal *9* (*2*), 1182-1183. 10.1017/S1431927603445911.
45. Punjani, A., Rubinstein, J.L., Fleet, D.J., and Brubaker, M.A. (2017). cryoSPARC: algorithms for rapid unsupervised cryo-EM structure determination. Nat Methods *14*, 290-296. 10.1038/nmeth.4169.
46. Punjani, A., Zhang, H., and Fleet, D.J. (2020). Non-uniform refinement: adaptive regularization improves single-particle cryo-EM reconstruction. Nat Methods *17*, 1214-1221. 10.1038/s41592-020-00990-8.
47. Bepler, T., Kelley, K., Noble, A.J., and Berger, B. (2020). Topaz-Denoise: general deep denoising models for cryoEM and cryoET. Nature communications *11*. ARTN 5208
10.1038/s41467-020-18952-1.
48. Bepler, T., Morin, A., Rapp, M., Brasch, J., Shapiro, L., Noble, A.J., and Berger, B. (2019). Positive-unlabeled convolutional neural networks for particle picking in cryo-electron micrographs. Nature Methods *16*, 1153-+. 10.1038/s41592-019-0575-8.
49. Croll, T.I. (2018). : a physically realistic environment for model building into low-resolution electron-density maps. Acta Crystallogr D *74*, 519-530. 10.1107/S2059798318002425.
50. Meng, E.C., Goddard, T.D., Pettersen, E.F., Couch, G.S., Pearson, Z.J., Morris, J.H., and Ferrin, T.E. (2023). UCSF ChimeraX: Tools for structure building and analysis. Protein Sci *32*. ARTN e4792
10.1002/pro.4792.
51. Emsley, P., Lohkamp, B., Scott, W.G., and Cowtan, K. (2010). Features and development of Coot. Acta crystallographica. Section D, Biological crystallography *66*, 486-501. 10.1107/S0907444910007493
10.1107/S0907444910007493. Epub 2010 Mar 24.</p>.
52. Afonine, P.V., Poon, B.K., Read, R.J., Sobolev, O.V., Terwilliger, T.C., Urzhumtsev, A.,

and Adams, P.D. (2018). Real-space refinement in PHENIX for cryo-EM and crystallography. Acta Crystallogr D Struct Biol *74*, 531-544. 10.1107/S2059798318006551.

53. Norby, J.G. (1988). Coupled assay of Na+,K+-ATPase activity. Methods in enzymology *156*, 116-119.